

REPORT DOCUMENTATION PAGE

Form Approved
OMB No. 0704-0188

Public reporting burden for this collection of information is estimated to average 1 hour per response, including the time for reviewing instructions, searching existing data sources, gathering and maintaining the data needed, and completing and reviewing the collection of information. Send comments regarding this burden estimate or any other aspect of this collection of information, including suggestions for reducing this burden, to Washington Headquarters Services, Directorate for Information Operations and Reports, 1215 Jefferson Davis Highway, Suite 1204, Arlington, VA 22202-4302, and to the Office of Management and Budget, Paperwork Reduction Project (0704-0188), Washington, DC 20503.

1. AGENCY USE ONLY (Leave blank)		2. REPORT DATE 3/7/97	3. REPORT TYPE AND DATES COVERED Final Technical	
4. TITLE AND SUBTITLE Receptivity Theory in Compressible Jet Flow Control			5. FUNDING NUMBERS F49620-94-1-0206	
6. AUTHOR(S) Edward J. Kerschen, Professor			AFOSR-TR-97 0160	
7. PERFORMING ORGANIZATION NAME(S) AND ADDRESS(ES) Department of Aerospace and Mechanical Engineering The College of Engineering and Mines The University of Arizona Tucson, Arizona 85721				
9. SPONSORING/MONITORING AGENCY NAME(S) AND ADDRESS(ES) AFOSR/NA 110 Duncan Avenue, Suite B115 Bolling AFB, DC 20332-8080			10. SPONSORING/MONITORING AGENCY REPORT NUMBER 94-1-0206	
11. SUPPLEMENTARY NOTES				
12a. DISTRIBUTION/AVAILABILITY STATEMENT Approved for public release Distribution is unlimited			12b. CODE 19970602 129	
13. ABSTRACT An analysis is presented for the generation of shear-layer instability waves by localized sources close to and far from the trailing edge. The frequency is assumed low enough that the shear layer can be represented by a vortex sheet, and the solution is developed using the Wiener-Hopf technique. Actuators (sources) on both surfaces of the splitter plate, and in the quiescent fluid just outside the shear layer, are considered. Results are presented for both subsonic and supersonic Mach numbers. Actuators on the stream side of the splitter plate are found to be more effective in generating shear-layer instability waves than actuators on the side adjacent to the quiescent fluid. The receptivity is highest for actuators located very near the trailing edge. For upstream actuators located on or near the splitter plate surface, the receptivity level decreases algebraically with distance from the trailing edge. In contrast, for actuators located just outside the shear layer downstream of the trailing edge, the receptivity level decreases exponentially with distance from the trailing edge.				
14. SUBJECT TERMS			15. NUMBER OF PAGES 27	
			16. PRICE CODE	
17. SECURITY CLASSIFICATION OF REPORT Unclassified	18. SECURITY CLASSIFICATION OF THIS PAGE Unclassified	19. SECURITY CLASSIFICATION OF ABSTRACT Unclassified	20. LIMITATION OF ABSTRACT UL	

RECEPTIVITY THEORY IN COMPRESSIBLE FLOW JET CONTROL

E. J. Kerschen

Department of Aerospace and Mechanical Engineering
The University of Arizona

Final Report
AFOSR Grant F49620-94-1-0206

February 1997

Abstract

An analysis is presented for the generation of shear-layer instability waves by localized sources close to and far from the trailing edge. The frequency is assumed low enough that the shear layer can be represented by a vortex sheet, and the solution is developed using the Wiener-Hopf technique. Actuators (sources) on both surfaces of the splitter plate, and in the quiescent fluid just outside the shear layer, are considered. Results are presented for both subsonic and supersonic Mach numbers. Actuators on the stream side of the splitter plate are found to be more effective in generating shear-layer instability waves than actuators on the side adjacent to the quiescent fluid. The receptivity is highest for actuators located very near the trailing edge. For upstream actuators located on or near the splitter plate surface, the receptivity level decreases algebraically with distance from the trailing edge. In contrast, for actuators located just outside the shear layer downstream of the trailing edge, the receptivity level decreases exponentially with distance from the trailing edge.

1 Introduction

Through the excitation of instability waves in jet shear layers, important features of jet flows may be controlled. These include thrust vectoring, modifications to jet mixing, and the suppression of noise and infrared signatures. In order to develop optimum approaches for the excitation of shear-layer instability waves in jets, the receptivity mechanisms by which these waves are generated must be understood, and the relative effectiveness of different

excitation methods must be quantified. This report presents a theoretical study of shear-layer receptivity processes of relevance to jet control. Related experimental and computational studies developed under AFOSR contract F49620-94-C-0029 are discussed in Parekh et al [1] and Cain [2], respectively.

To produce receptivity, external disturbances must induce motion within the shear layer that matches the frequency-wavelength combination of the instability wave. For shear layers, the trailing edge (or nozzle lip) often plays an important role in the transfer of energy from the spatial spectrum of the external disturbance to that of the instability wave field. Thus, it is essential that the influence of the trailing edge be included in the theoretical analyses. The theoretical formulations then take the form of two-part boundary-value problems, the no-penetration condition being applicable on the nozzle surface ($x < 0$), while continuity of pressure and continuity of particle displacement conditions apply downstream of the nozzle lip ($x > 0$).

The parameter space throughout which jet control is desirable is quite large, containing a wide range of Mach numbers and temperature ratios. In order to obtain a global picture of shear layer receptivity behavior throughout this parameter space, the development of a simplified model is desirable. Since the boundary layer at a nozzle exit is usually quite thin, and low-frequency instability waves have the most potential for downstream growth, a focus on the case of thin shear layers appears profitable. In this report we assume that the Strouhal number $S = \omega\delta/U$ is small enough that the vortex-sheet approximation for the shear layer is applicable. Here ω is the frequency of the instability wave, δ is a measure of the thickness of the shear layer, and U is the speed of the jet.

Previous theoretical studies of unsteady trailing-edge interactions utilizing the vortex-sheet approximation were presented by Morgan [3], Munt [4][5], and Cargill [6]. Morgan considered an external point source in a supersonic flow, but focused on the scattering of the acoustic field rather than the generation of an instability wave. Similarly, Munt and Cargill focused on transmission of a sound wave out a circular jet pipe. The present report is focused on instability wave generation. We develop a two-dimensional analysis which considers only a single splitter plate, corresponding to a jet of semi-infinite width. A receptivity analysis for a circular jet, with an acoustic source related to the screech problem, is presented in Pal [7] and Bower and Pal [8].

In section 2, the theoretical model is formulated as a two-part mixed boundary-value problem. In section 3, the Wiener-Hopf technique is utilized to obtain the solution to this mixed boundary-value problem. Receptivity Coefficients for a range of flow speeds (incompressible, subsonic and supersonic) and actuator locations are presented in section 4.

2 Formulation

The basic length scale governing the dynamics of the receptivity process is the instability wavelength λ_v . In the vicinity of the nozzle lip, the thickness δ of the jet shear layer is generally quite thin compared to λ_v , corresponding to the limit $S = \omega\delta/U \ll 1$. In this limit, the analysis of the instability wave generation can be simplified by replacing the finite-

thickness shear layer by a vortex sheet. (Formally, the vortex-sheet model is obtained by applying a low-frequency approximation to the equations governing a finite-thickness shear layer.) Often, the nozzle lip is also thin compared to the instability wavelength. In this situation, the nozzle surface can be approximated by a rigid sheet of zero thickness.

In the vicinity of the nozzle lip, the amplitudes of the impinging sound field and the generated instability wave are usually quite small compared to the mean flow speed. Therefore, the unsteady motion can be analyzed as a small perturbation to the mean flow field. In order to further simplify the modeling of the receptivity process, we introduce a few additional assumptions. First, we consider a two-dimensional nozzle whose width is large compared to the instability wavelength. The receptivity of the shear layers on the two boundaries of the jet can then be analyzed separately. Second, we assume that the nozzle surface extends upstream at constant area for a distance of several wavelengths. In this situation, the nozzle surface can be approximated by a rigid, zero-thickness sheet that extends to upstream infinity. Finally, for the case of a supersonic jet we assume that the jet is perfectly expanded, so that the jet flow leaves the nozzle without undergoing an expansion or compression process. The above assumptions may seem somewhat restrictive, but are motivated by the desire for a relatively simple theory which is applicable to a wide range of parameter space. Once a basic theory is in place, various refinements to the modeling could be explored.

Concentrating on a single shear layer of the jet, the nozzle surface is represented by a rigid, semi-infinite sheet, extending along the negative x' axis from the origin to negative infinity, as illustrated in figure 1. The nozzle lip (or trailing edge) is located at the origin. The mean flow in the jet is assumed to be uniform upstream and downstream of the nozzle exit. In the present work, we assume that the jet exhausts into a quiescent medium. The mean flow is then given by

$$\mathbf{u}_0 = \begin{cases} 0, & y' > 0 \\ U \mathbf{e}_{x'}, & y' < 0 \end{cases} \quad (1)$$

the regions $y' < 0$ and $y' > 0$ corresponding to the jet stream and the surrounding quiescent medium, respectively. Downstream of the trailing edge, the jet boundary ($y' = 0$) takes the form of a vortex sheet. The mean pressure p_0 is the same inside and outside the jet, while the temperature T_{0-} and density ρ_{0-} inside the jet may be different than the corresponding values T_{0+} and ρ_{0+} outside the jet. The sound speeds c_{0-} and c_{0+} are given by the perfect gas formula $c = \sqrt{\gamma p / \rho}$, where γ is the ratio of specific heats. The relation $\rho_{0-} c_{0-}^2 = \rho_{0+} c_{0+}^2$ follows as a consequence of the pressure p_0 being the same inside and outside the jet. The base flow Mach number within the jet is $M_- = U / c_{0-}$. It proves convenient to also introduce a Mach number, $M_+ = U / c_{0+}$, based on the speed of sound outside the jet. However, it must be remembered that the base flow vanishes outside the jet; M_+ is simply a parameter that is introduced in order to express the equations in a convenient form.

Linearizing the governing equations about the base state (1), the flow perturbations $(p_-, \rho_-, \mathbf{u}_-)$ within the jet satisfy the equations

$$\frac{D_0 p_-}{Dt'} + \rho_0 c_0^2 \nabla \cdot \mathbf{u}_- = 0, \quad (2a)$$

$$\rho_{0-} \frac{D_0 \mathbf{u}_-}{Dt'} = -\nabla p_-, \quad (2b)$$

$$\rho_- = \frac{p_-}{c_{0-}^2}, \quad (2c)$$

where $\mathbf{u}_- = (u_-, v_-)$, t' is time, and $D_0/Dt' = \partial/\partial t' + U\partial/\partial x'$ is the substantial derivative with respect to the mean flow. The flow perturbations $(p_+, \rho_+, \mathbf{u}_+)$ outside the jet satisfy (2) with U set to zero and ρ_{0-} , c_{0-} replaced by ρ_{0+} , c_{0+} .

On the nozzle surface ($x' < 0$), the perturbation flow satisfies the no-penetration boundary condition

$$v_{\pm}|_{y'=0} = 0. \quad (3)$$

Downstream of the trailing edge ($x' > 0$), the perturbation flow satisfies two matching conditions across the vortex sheet that forms the boundary of the jet. These matching conditions are continuity of pressure,

$$p_+|_{y'=0} = p_-|_{y'=0}, \quad (4)$$

and continuity of particle displacement,

$$v_+|_{y'=0} = \frac{\partial h'}{\partial t'}, \quad v_-|_{y'=0} = \frac{\partial h'}{\partial t'} + U \frac{\partial h'}{\partial x'}, \quad (5)$$

where $h'(x', t')$ is the displacement of the vortex sheet and linearization has been utilized to transfer the conditions from the instantaneous position $y' = h'(x', t')$ to the mean surface $y' = 0 \pm$. The Sommerfeld radiation condition applies at infinity.

Since the base flow is irrotational outside of the vortex sheet, the flow perturbations can be expressed in terms of velocity potentials, say ϕ_+ and ϕ_- . Setting $\mathbf{u}_- = \nabla \phi_-$, (2b) can be integrated to obtain

$$p_- = -\rho_{0-} \frac{D_0 \phi_-}{Dt'}. \quad (6)$$

Equations (2a) and (2b) can then be combined to yield the convected wave equation,

$$\nabla^2 \phi_- - \frac{1}{c_{0-}^2} \frac{D_0^2 \phi_-}{Dt'^2} = 0. \quad (7)$$

The corresponding flow perturbations outside the jet satisfy (7) with U set to zero and ρ_{0-} , c_{0-} replaced by ρ_{0+} , c_{0+} .

The next step in the analysis is to represent the field as the sum of an 'incident field', due to an actuator or other source, and a 'scattered field', produced by the interaction of the incident field with the shear layer and the trailing edge. For an actuator or source in the ambient region ($y' > 0$), the function $\phi_+(x', y', t')$ is separated into incident and scattered components, $\phi_{i+}(x', y', t')$ and $\phi_{s+}(x', y', t')$, while $\phi_-(x', y', t')$ contains only a scattered component. We also consider the case of an actuator on the inside surface of the nozzle ($y \rightarrow 0-$). For this case $\phi_-(x', y', t')$ is separated into incident and scattered components. We choose

to illustrate the analysis for the case of a point source in the ambient region ($y' > 0$). After developing the analysis for this case, the differences that arise in the case of an actuator on the internal surface of the nozzle will be discussed.

The solutions for ϕ_- and ϕ_+ are developed using a Fourier transform with respect to the streamwise coordinate. However, since the boundary conditions in the region $x' < 0$ are different than those in the region $x' > 0$, a special technique is required. We have developed the solutions using the Wiener-Hopf technique [9]. In the Wiener-Hopf technique, Fourier transform methods are combined with analytic continuation in the complex wavenumber plane to determine the solution. A transform method is particularly well suited for determination of the (complex) amplitude of the instability wave, since the instability wave appears as a pole of the solution in transform space. The amplitude of the instability wave is found by evaluating the residue associated with this pole, a much simpler task than the full evaluation of the inverse transform.

Solutions have been developed for incompressible, subsonic and supersonic flows. There are significant differences in the physics of the unsteady flow for these three cases, which are reflected in the structure of the singularities in the complex wavenumber plane. The singularities for the incompressible, subsonic and supersonic cases are illustrated in figures 2a, 2b and 2c, respectively. Due to these differences in the singularity structure, differences in the details of the Wiener-Hopf analysis arise. For the sake of illustration, we concentrate on the supersonic flow case. After the analysis for this case has been developed, the differences which arise for subsonic and incompressible flows will be discussed.

Thus, consider the case of a localized, time-harmonic volume source of dimensional strength q' in the ambient region at position (x'_0, y'_0) . The source is represented by introducing an inhomogeneous term

$$q' \delta(x' - x'_0) \delta(y' - y'_0) \exp(-i\omega t'),$$

on the right-hand side of the wave equation (7) (with ρ_{0+}, ρ_{0-} and $U = 0$) which $\phi_+(x, y)$ satisfies.

With the assumptions that the splitter plate (or nozzle lip) extends to upstream infinity and that both the splitter plate and shear layer are of infinitesimal thickness, the problem does not contain a geometrical length scale. The hydrodynamic length scale U/ω can therefore be used for nondimensionalization. Upon extraction of the harmonic time dependence, the frequency then does not appear explicitly in the resulting equations, so that a single (nondimensional) solution applies at all frequencies for which the vortex-sheet approximation is applicable.

Setting

$$t = \omega t', \quad x = \frac{\omega x'}{U}, \quad y = \frac{\omega y'}{U} \quad (8)$$

and

$$\phi_+ = q' g_+(x, y) e^{-it}, \quad \phi_- = q' g_-(x, y) e^{-it}, \quad (9)$$

the reduced potentials $g_+(x, y)$ and $g_-(x, y)$ satisfy the differential equations

$$\frac{\partial^2 g_+}{\partial x^2} + \frac{\partial^2 g_+}{\partial y^2} + M_+^2 g_+ = \delta(x - x_0)\delta(y - y_0), \quad (10a)$$

$$\frac{\partial^2 g_-}{\partial x^2} + \frac{\partial^2 g_-}{\partial y^2} + M_-^2 \left(1 + i \frac{\partial}{\partial x}\right)^2 g_- = 0. \quad (10b)$$

On the nozzle surface ($x < 0$), the reduced potentials satisfy the homogeneous boundary conditions

$$\left. \frac{\partial g_+}{\partial y} \right|_{y=0+} = 0, \quad \left. \frac{\partial g_-}{\partial y} \right|_{y=0-} = 0, \quad (11)$$

while for $x > 0$ the pressure and particle-displacement matching conditions across the vortex sheet take the form

$$M_+^2 g_+|_{y=0+} = M_-^2 \left(1 + i \frac{\partial}{\partial x}\right) g_-|_{y=0-}, \quad (12a)$$

$$\left(1 + i \frac{\partial}{\partial x}\right) \left. \frac{\partial g_+}{\partial y} \right|_{y=0+} = \left. \frac{\partial g_-}{\partial y} \right|_{y=0-}. \quad (12b)$$

Finally, the modified potentials $g_+(x, y)$ and $g_-(x, y)$ also satisfy the appropriate form of the Sommerfeld radiation condition. In the following section, the Wiener-Hopf technique is utilized to obtain the solutions for g_+ and g_- .

3 Solution

In this section, we develop the solution for the case of a supersonic shear layer excited by a time-harmonic source in the ambient field. Equations (10a - 12) for the reduced potential functions $g_+(x, y)$ and $g_-(x, y)$ form a mixed boundary-value problem, since the boundary conditions (12) that apply on $x > 0$ are different than the conditions (11) that apply on $x < 0$. Due to the presence of the mixed boundary conditions, the solution of (10a - 12) requires a special technique. In this report, the solution is developed utilizing the Wiener-Hopf technique [9]. In the Wiener-Hopf technique, Fourier transform methods are combined with analytic continuation in the complex wavenumber plane in order to determine the solution. A transform solution is particularly well suited for determination of the (complex) amplitude of the instability wave, since the instability wave appears as a pole of the solution in transform space. The amplitude of the instability wave is found by evaluating the residue associated with this pole, a much simpler task than the full evaluation of the inverse transform.

The Fourier transform $G(\lambda, y)$ and its inverse are defined as

$$G(\lambda, y) = \int_{-\infty}^{\infty} g(x, y) \exp(i\lambda x) dx, \quad g(x, y) = \frac{1}{2\pi} \int_{-\infty}^{\infty} G(\lambda, y) \exp(-i\lambda x) d\lambda. \quad (13)$$

Applying the transform to (10a), solving the resulting ordinary differential equation in y and noting that the solution must remain bounded as $y \rightarrow \infty$, we obtain

$$G_+(\lambda, y) = C_+(\lambda) \exp(-\mu_+(\lambda)y) - \frac{1}{2\mu_+(\lambda)} \exp(i\lambda x_0 - \mu_+(\lambda)|y - y_0|), \quad (14)$$

where

$$\mu_+(\lambda) = \sqrt{\lambda^2 - M_+^2}. \quad (15)$$

The first term in (14) is a complementary solution to the homogeneous equation (corresponding to the scattered potential ϕ_{s+}), while the second term is a particular solution (corresponding to the incident field ϕ_{i-}). The function $\mu_+(\lambda)$ corresponds to the branch of the square root that is real and positive as $\lambda \rightarrow +\infty$ along the real λ axis. In order to satisfy the Sommerfeld radiation condition, the branch points of μ_+ at $\lambda = \pm M_+$ are assumed to lie just above and below the real λ axis, respectively, the inversion contour in (13) being the real λ axis. The branch cuts extending from $\pm M_+$ are illustrated in figure 2c.

Similarly, applying the transform to (10b) and noting that the solution must remain bounded as $y \rightarrow -\infty$, we obtain the corresponding result

$$G_-(\lambda, y) = C_-(\lambda) \exp(\mu_-(\lambda)y), \quad (16)$$

where

$$\begin{aligned} \mu_-(\lambda) &= \sqrt{\lambda^2 - M_-^2(1 + \lambda)^2} \\ &= -i\beta\sqrt{(\lambda - M_1)(\lambda - M_2)}, \end{aligned} \quad (17)$$

and $\beta = \sqrt{M_-^2 - 1}$, the second form of $\mu_-(\lambda)$ exposing the branch points at

$$M_1 = \frac{-M_-}{M_- + 1} \quad \text{and} \quad M_2 = \frac{-M_-}{M_- - 1}, \quad (18)$$

The branch points at $\lambda = M_1$ and M_2 lie just below the real λ axis and the branch cuts extend down into the lower half-plane, as illustrated in figure 2c. The difference in the locations of the branch points and branch cuts for μ_- as compared to those for μ_+ is related to the lack of upstream influence in a supersonic stream. The function μ_- is real positive for real values of λ in the range $M_2 < \lambda < M_1$; μ_- is negative imaginary for $\lambda > M_1$ and positive imaginary for $\lambda < M_2$.

Next consider the application of the Fourier transform (13) to the boundary conditions. Since the boundary conditions are specified only on the half-ranges $x > 0$ and $x < 0$, while the transform involves the full range $-\infty < x < \infty$, we must introduce some half-known functions in order to apply the transform. The pressure matching condition (12a) applies on $x > 0$. Thus, we set

$$M_+^2 g_+(x, 0) - M_-^2 \left(1 + i \frac{\partial}{\partial x}\right) g_-(x, 0) = u(x), \quad (19)$$

where $u(x)$ is a function that is half-known since $u(x) = 0$ for $x > 0$. Applying the transform (13) over the full range $-\infty < x < \infty$, and utilizing (14) and (16), we obtain

$$M_+^2 C_+(\lambda) - M_+^2 \frac{\exp(i\lambda x_0 - \mu_+(\lambda)y_0)}{2\mu_+(\lambda)} - M_-^2(1 + \lambda)C_-(\lambda) = U^-(\lambda), \quad (20)$$

where $U^-(\lambda)$ is the Fourier transform of $u(x)$. The superscript $(\cdot)^-$ on $U(\lambda)$ denotes that this function is analytic in the lower half of the complex λ -plane ($Im[\lambda] < 0$), a property which follows from the fact that $u(x) = 0$ for $x > 0$. In the Wiener-Hopf nomenclature, such functions are called minus functions.

Next consider the particle-displacement matching condition (12b). This vortex-sheet condition is obviously satisfied on $x > 0$, and it is also satisfied on $x < 0$ by virtue of the hard-wall boundary condition (11). Thus, we can transform this condition on the full range $-\infty < x < \infty$ to obtain

$$(1 + \lambda) \left. \frac{\partial G_+}{\partial y} \right|_{y=0+} - \left. \frac{\partial G_-}{\partial y} \right|_{y=0-} = 0. \quad (21)$$

Substituting in the expressions (14, 16), we obtain

$$(1 + \lambda) \left[-\mu_+(\lambda)C_+(\lambda) - \frac{1}{2} \exp(i\lambda x_0 - \mu_+(\lambda)y_0) \right] - \mu_-(\lambda)C_-(\lambda) = 0. \quad (22)$$

Next, we combine (20) and (22) in a form that involves the transforms of two 'half-known' functions. One of these is $U^-(\lambda)$, the transform of $u(x)$. To identify a function that is analytic in the upper half plane, note that the disturbance cannot penetrate into the region $x < 0$ within the supersonic jet. Thus $\phi_-(x, 0)$ is zero for $x < 0$, and $C_-(\lambda)$ is a 'plus' function. Now $\mu_-(\lambda)$ is also a plus function, since both branch cuts lie in the lower half plane (see figure 2c). It proves convenient to choose $d(x) = \partial g_- / \partial y|_{y=0-}$ as the second half-known function; its transform is

$$D^+(\lambda) = \mu_-(\lambda)C_-(\lambda) \quad (23)$$

where the superscript $(\cdot)^+$ on $D(\lambda)$ denotes that this is a plus function, i.e., a function that is analytic in the upper half of the complex λ plane ($Im[\lambda] > 0$). (Later, it will be seen that $d(x)$ contains an instability wave component which exhibits exponential growth as $x \rightarrow \infty$, requiring a slight modification to the definitions of the upper and lower halves of the complex λ plane.)

To apply the analytic continuation argument of the Wiener-Hopf technique, we require a single equation in which the only unknown quantities are the two half-analytic functions, $U^-(\lambda)$ and $D^+(\lambda)$. This is achieved by using (21) to eliminate $C_+(\lambda)$ from the pressure condition (20). Upon rearrangement we obtain

$$\frac{-iM_-^2}{\beta} \frac{1}{K(\lambda)} \frac{(\lambda + n)}{(1 + \lambda)} D^+(\lambda) = U^-(\lambda) + M_+^2 \frac{\exp(i\lambda x_0 - \mu_+(\lambda)y_0)}{\mu_+(\lambda)} \quad (24)$$

where

$$K(\lambda) = \frac{iM_-^2}{\beta} \frac{(\lambda + n)\mu_+(\lambda)\mu_-(\lambda)}{M_-^2(1 + \lambda)^2\mu_+(\lambda) + M_+^2\mu_-(\lambda)} \quad (25)$$

Equation (24) has the standard form of a Wiener-Hopf equation. It contains two unknown functions, $D^+(\lambda)$ and $U^-(\lambda)$, which are analytic in the upper and lower halves of the complex λ plane, respectively. The kernel function $K(\lambda)$ contains the singularities of $\mu_+(\lambda)$ and $\mu_-(\lambda)$; the branch point of $\mu_+(\lambda)$ at $\lambda = M_+$ lies in the upper half plane, while the branch point of $\mu_-(\lambda)$ at $\lambda = -M_+$ and the branch points of $\mu_-(\lambda)$ at $\lambda = M_1$ and M_2 lie in the lower half-plane (see figure 2c). The denominator of $K(\lambda)$ vanishes at $\lambda = -n$ where n is the wavenumber of the instability wave. This zero is not a pole of $K(\lambda)$ because of the factor $(\lambda + n)$ in the numerator. Extraction of this factor proves convenient for displaying the pole corresponding to the instability wave. The additional factors in the definition (25) of $K(\lambda)$ have been included to insure that $K(\lambda)$ approaches one as $\lambda \rightarrow \infty$; this is advantageous for the subsequent separation of $K(\lambda)$ into the product of a plus function and a minus function.

In order to apply the analytic continuation argument of the Wiener-Hopf technique, (24) must be rearranged so that one side is analytic in the upper half-plane, while the other side is analytic in the lower half-plane. We begin by separating $K(\lambda)$ into multiplicative factors

$$K(\lambda) = K^+(\lambda)K^-(\lambda),$$

where $K^+(\lambda)$ is analytic in the upper half-plane and $K^-(\lambda)$ is analytic in the lower-half plane. The calculation of $K^+(\lambda)$ and $K^-(\lambda)$ is discussed in the Appendix. Taking $K^-(\lambda)$ to the left-hand side of the equation, we have

$$\frac{-iM_-^2}{\beta} \frac{1}{K^+(\lambda)} \frac{(\lambda + n)}{(1 + \lambda)} D^+(\lambda) = U^-(\lambda)K^-(\lambda) + M_+^2 K^-(\lambda) \frac{\exp(i\lambda x_0 - \mu_+(\lambda)y_0)}{\mu_+(\lambda)} \quad (26)$$

It will be seen in a moment that the pole on the right-hand side of the equation at $\lambda = -1$ is interpreted to lie in the lower half-plane. Thus, the left-hand side of (26) is analytic in the upper half-plane, while the first term on the right-hand side is analytic in the lower half-plane. However, the second term on the right-hand side is a mixed function, containing singularities in both half-planes.

In order to complete the Wiener-Hopf separation, an additive split of the mixed function must be performed. We set

$$H(\lambda) = K^-(\lambda) \frac{\exp(i\lambda x_0 - \mu_+(\lambda)y_0)}{\mu_+(\lambda)} = H^+(\lambda) + H^-(\lambda) \quad (27)$$

where the calculation of $H^+(\lambda)$ and $H^-(\lambda)$ is discussed in the Appendix. Substituting (27) and taking the term involving $H^+(\lambda)$ to the left-hand side of (26), we obtain

$$\frac{-iM_-^2}{\beta} \frac{1}{K^+(\lambda)} \frac{(\lambda + n)}{(1 + \lambda)} D^+(\lambda) - M_+^2 H^+(\lambda) = U^-(\lambda)K^-(\lambda) + M_+^2 H^-(\lambda) - E(\lambda) \quad (28)$$

The left-hand side of (28) is analytic in the upper half-plane, while the right-hand side is analytic in the lower half-plane. The two sides are equal in the strip of overlap between the two half-planes, and therefore by analytic continuation define an entire function $D(\lambda)$ which is analytic over the whole λ plane.

The entire function $E(\lambda)$ is determined with the aid of Liouville's theorem [9], which states that a function which is analytic in the entire plane and bounded at infinity must be a constant. To find this constant, we examine the behavior of the minus and plus sides of (28) as λ approaches infinity in the respective half-planes. The functions $K^+(\lambda)$ and $K^-(\lambda)$ both approach one as λ approaches infinity in the respective half-planes. The behavior of $U^-(\lambda)$ as $\lambda \rightarrow \infty$ in the lower half-plane is related to the behavior of $u(x)$ as $x \rightarrow 0^-$, while the behavior of $D^+(\lambda)$ as $\lambda \rightarrow \infty$ in the upper half-plane is related to the behavior of $d(x)$ as $x \rightarrow 0^+$. The behaviors of $u(x)$ and $d(x)$ near the origin are constrained by the requirement for acceptable behavior of the flow field in the vicinity of the trailing edge. These constraints are called 'edge conditions' in the Wiener-Hopf literature.

In the present case, the edge conditions are determined by requiring that the solution satisfy the unsteady Kutta condition [10]. For the familiar subsonic flow case, in the absence of the Kutta condition the inviscid velocity field would become infinite in the vicinity of the trailing edge; the corresponding unsteady displacement of the vortex sheet would have the form $h \propto x^{1/2}e^{-it}$. With the imposition of the Kutta condition, the transverse velocities inside and outside the jet vanish at the trailing edge, the pressure has the same value on the upper and lower surfaces at the trailing edge, and $h \propto x^{3/2}e^{-it}$.

The behavior of the flow field in the vicinity of the trailing edge is quite different for a supersonic flow [3], [10], [11]. In this case, the flow field corresponding to the application of an unsteady 'Kutta condition' has $h \propto xe^{-it}$. From (5), the corresponding transverse velocity outside the jet has behavior $v_+ \propto xe^{-it}$, while inside the jet the transverse velocity is discontinuous at the trailing edge; $v_-|_{y=0} = 0$ for $x < 0$, while the leading behavior for $x > 0$ is $v_-|_{y=0} \propto e^{-it}$. Essentially, the unsteady pressure fluctuation for a supersonic jet can have different values inside and outside the nozzle, the adjustment at the nozzle lip taking the form of a linear expansion or compression wave, leading to a vortex sheet deflection that is locally a linear function of x .

To apply these results to the solution of the present Wiener-Hopf problem, note that the function $u(x)$ is related to the pressure jump across the nozzle surface (see (12a) and (19). The unsteady pressure difference across the nozzle surface must be finite, which implies that $u(x) \rightarrow c_1$ as $x \rightarrow 0^-$. It can then be shown that $U^-(\lambda) \propto \lambda^{-1}$ as $\lambda \rightarrow \infty$ in the lower half-plane. A similar argument shows that $d(x) \rightarrow c_2$ as $x \rightarrow 0^+$, implying that $D^+(\lambda) \propto \lambda^{-1}$ as $\lambda \rightarrow \infty$ in the upper half-plane. The functions $H^+(\lambda)$ and $H^-(\lambda)$ also approach zero as $\lambda \rightarrow \infty$ in the respective half-planes. Thus, both sides of (28) approach zero for large λ , and the entire function $E(\lambda)$ is identically zero. The plus and minus sides of (28) can then be set to zero separately, leading to the results

$$U^-(\lambda) = -\frac{M_+^2 H^-(\lambda)}{K^-(\lambda)}, \quad (29)$$

$$D^+(\lambda) = i\beta \frac{M_+^2 (1+\lambda)}{M_-^2 (\lambda+n)} H^+(\lambda) K^+(\lambda). \quad (30)$$

Then from (19) and (22) we obtain

$$C_+(\lambda) = -i\beta \frac{M_+^2 H^+(\lambda) K^+(\lambda)}{M_-^2 (\lambda+n)\mu_+(\lambda)} - \frac{1}{2} \frac{\exp(i\lambda x_0 - \mu_+(\lambda)y_0)}{\mu_+(\lambda)}, \quad (31)$$

$$C_-(\lambda) = i\beta \frac{M_+^2 (1+\lambda) H^+(\lambda) K^+(\lambda)}{M_-^2 (\lambda+n)\mu_+(\lambda)}. \quad (32)$$

The inverse transforms can then be evaluated, leading to

$$\phi_+(x, y) = -\frac{i\beta M_+^2}{2\pi M_-^2} \int_{-\infty}^{\infty} \frac{H^+(\lambda) K^+(\lambda)}{(\lambda+n)\mu_+(\lambda)} \exp(i\lambda x - \mu_+(\lambda)y) d\lambda \quad (33)$$

$$-\frac{i}{4} H_0^{(1)}(M_+ [(x-x_0)^2 + (y-y_0)^2]^{1/2})$$

$$-\frac{i}{4} H_0^{(1)}(M_+ [(x-x_0)^2 + (y+y_0)^2]^{1/2}),$$

$$\phi_-(x, y) = \frac{i\beta M_+^2}{2\pi M_-^2} \int_{-\infty}^{\infty} \frac{H^+(\lambda) K^+(\lambda) (1+\lambda)}{(\lambda+n)\mu_-(\lambda)} \exp(i\lambda x + \mu_-(\lambda)y) d\lambda. \quad (34)$$

Our main interest is in the amplitude of the instability wave component of the solution. The instability wave component can be calculated by simply evaluating the residue contribution for the pole at $\lambda = -n$. Denoting the instability wave component with a subscript $(\cdot)_v$, we have

$$\phi_{v+} = -\frac{\beta M_+^2}{M_-^2} H^+(-n) K^+(-n) \frac{1}{m_+} \exp(inx - m_+ y), \quad (35)$$

$$\phi_{v-} = \frac{\beta M_+^2}{M_-^2} H^+(-n) K^+(-n) \frac{(1-n)}{m_-} \exp(inx + m_- y), \quad (36)$$

where $m_+ = \mu_+(-n)$ and $m_- = \mu_-(-n)$, where n is the root of the vortex-sheet dispersion relationship. The dimensional pressure and velocity fields for the instability wave are then

$$p'_{v+} = -i\rho_0 \omega q' \frac{\beta M_+^2}{M_-^2} H^+(-n) K^+(-n) \frac{1}{m_+} \exp(inx - m_+ y - it), \quad (37)$$

$$u'_{v+} = -i \frac{\omega q'}{U} \frac{\beta M_+^2}{M_-^2} H^+(-n) K^+(-n) \frac{n}{m_+} \exp(inx - m_+ y - it), \quad (38)$$

$$v'_{v+} = \frac{\omega q'}{U} \frac{\beta M_+^2}{M_-^2} H^+(-n) K^+(-n) \exp(inx - m_+ y - it), \quad (39)$$

in the region outside the jet ($y > 0$), and the corresponding expressions inside the jet ($y < 0$) are

$$p'_{v-} = i\rho_0 \omega q' \frac{\beta M_+^2}{M_-^2} H^+(-n) K^+(-n) \frac{(1-n)^2}{m_-} \exp(inx + m_- y - it), \quad (40)$$

$$u'_{v-} = i \frac{\omega q'}{U} \frac{\beta M_+^2}{M_-^2} H^+(-n) K^+(-n) \frac{(1-n)n}{m_-} \exp(inx + m_-y - it), \quad (41)$$

$$v'_{v-} = \frac{\omega q'}{U} \frac{\beta M_+^2}{M_-^2} H^+(-n) K^+(-n) (1-n) \exp(inx + m_-y - it). \quad (42)$$

It is convenient to present the result for the (complex) amplitude of the instability wave in terms of a Receptivity Coefficient, which is a measure of the efficiency with which the external forcing generates the instability wave. Note that the natural scaling which appears in the expressions for the unsteady velocity field is $\omega q'/U$, roughly the magnitude of the velocity field of the point source at a distance corresponding to the natural length scale U/ω for the unsteady motion. Hence, we define the Receptivity Coefficient as

$$\Lambda = \frac{v'_{v+}|_{x=y=0}}{\omega q'/U \exp(-it)} \quad (43)$$

where $v'_{v+}|_{x=y=0}$ is the (dimensional) y -component of velocity just outside the vortex sheet, and q' is the (dimensional) strength of the point source. When expressed in this fashion, the Receptivity Coefficient becomes independent of frequency. Of course, the velocity v' near the trailing edge has hydrodynamic components in addition to the instability wave component, so that the total velocity field satisfies the unsteady Kutta condition. Using the expression for v'_{v+} given above, we obtain

$$\Lambda = \frac{\beta M_+^2}{M_-^2} H^+(-n) K^+(-n). \quad (44)$$

The calculation of $H^+(-n)$ and $K^+(-n)$ are discussed in the Appendix. Results for the Receptivity Coefficient are presented in the following section.

Before proceeding to a presentation of results for the Receptivity Coefficient, we briefly discuss differences which arise in the analysis for the other cases. For actuators on the inside surface of the nozzle, the analysis proceeds similarly except that the forcing is present in the region $y < 0$ and therefore it is g_- rather than g_+ that contains the particular solution. In addition, the case of the Wiener-Hopf splits, and also the physics of the unsteady flow in the vicinity of the trailing edge, is intimately connected to the singularity structure in the complex wavenumber plane. Figure 2 is an illustration of, the pole singularities and branch cuts which arise in three different regimes of incompressible, subsonic and supersonic flow.

The case of incompressible flow is shown in figure 2a. Two branch points are present, just above and below the origin, respectively. Also, a pair of poles occur, at $\lambda = -n$ and $-n^*$, respectively, where the $(\cdot)^*$ denotes the complex conjugate. The pole at $\lambda = -n$ corresponds to the exponentially growing instability wave while the pole at $-n^*$ is its exponentially damped counterpart. In order to obtain a causal solution, the transform inversion contour must pass above the pole at $\lambda = -n$. The presence of only two branch points leads to significant simplifications in the analysis, since the multiplicative split of $K(\lambda)$ can be obtained analytically. Evaluation of the subsequent additive split of $H(\lambda)$ depends on details of the actuator description, and in some cases can also be obtained analytically.

The singularity structure for subsonic flow is shown in figure 2b. Here four branch points arise, two in the upper half-plane and two in the lower. The branch points in the upper half-plane are associated with upstream-propagating disturbances inside and outside the stream, while the branch points in the lower half-plane are associated with the corresponding downstream-propagating disturbances. Two alternative choices for the branch cuts in the upper half-plane are shown in figure 2b. The vertical solid lines parallel to the imaginary axis are convenient for some applications, while for others it is most convenient to introduce a horizontal branch cut (dashed line) connecting the two branch points. Again, the pole at $\lambda = -n$ is associated with instability wave motion, the pole at $-n^*$ is its exponentially damped counterpart, and the inversion contour passes above $\lambda = -n$. The presence of four branch points significantly complicates the analysis. The multiplicative split of $K(\lambda)$ must be carried out by numerical integration in the complex λ plane, and the subsequent additive split of $H(\lambda)$ then becomes a nested double integral which must also be evaluated numerically. However, we still have the advantage that the analytical structure of the solution allows the instability-wave component of the unsteady motion to be extracted conveniently and precisely, as the residue of a pole of the inverse Fourier transform. In particular, the split function need only be evaluated at the location $\lambda = -n$ of the pole corresponding to the instability wave motion.

The singularity structure for supersonic flow is shown in figure 2c. Here four branch points are again present, but only one lies in the upper half plane. This change in the character of the branch points is associated with the lack of upstream influence in a supersonic stream. The instability wave pole at $\lambda = -n$ is still present, but its counterpart $-n^*$ has disappeared into a secondary Riemann sheet. The change in the singularity structure relative to the case of subsonic flow is reflected in a change in the character of the unsteady motion near the trailing edge. For a subsonic flow, the flow must leave the trailing edge tangential to the surface, corresponding to a local unsteady displacement of the vortex sheet which is proportional to $x^{3/2}$. This result, commonly called the unsteady Kutta condition, arises naturally from consideration of the 'edge conditions' in the Wiener-Hopf analysis. For a supersonic flow, the difference in branch cut structure is reflected in the edge conditions in such a way that the unsteady displacement of the vortex sheet is proportional to x . Thus, the unsteady supersonic flow deflects at a finite angle upon reaching the trailing edge, through alternating expansion and compression waves.

In the next section, we illustrate physical features of the shear layer receptivity process through selected examples. All cases presented in section 4 correspond to a cold flow, $T_- = T_+$. The quantity we focus on is the Receptivity Coefficient, a measure of the amplitude and phase of the instability wave relative to the amplitude and phase of the actuator motion.

4 Results

First consider the case of incompressible flow. In figure 3, we present results for the shear layer receptivity produced by a point source located at a point $(x_0, y_0) = r_0(\cos \theta_0, \sin \theta_0)$, in the quiescent fluid outside the stream. The quantity plotted is the magnitude $|\Lambda|$ of the

Receptivity Coefficient defined in the previous section.

In figures 3a-d, $|\Lambda|$ is plotted as a function of actuator angular location θ_0 , for four different fixed values of r_0 . At $r_0 = 0.1$, the receptivity level is almost independent of θ_0 , as expected. The position $r_0 = \frac{1}{2}\pi$ corresponds to a distance of $\frac{1}{4}$ the instability wavelength, and here there is a noticeable bias toward upstream positions ($\theta_0 \rightarrow \pi$). Note also the fairly sharp rise for very small θ_0 , where the actuator is nearly on top of the shear layer. This rise is related to the 'direct receptivity' of the actuator on the shear layer, as opposed to the receptivity path via the trailing edge. At $r_0 = \pi$, corresponding to a half-wavelength distance, the curve is starting to resemble the $r_0 \gg 1$ asymptotic behavior, shown as a dashed line. The local rise as $\theta_0 \rightarrow 0$ due to the direct receptivity is still visible, but the highest receptivity levels are associated with upstream positions ($\theta_0 > \frac{1}{2}\pi$). At $r_0 = 4\pi$, corresponding to two instability wavelengths, the curve is quite close to its asymptotic shape and the contribution from the direct receptivity is no longer visible.

In figures 4a-c, we illustrate the variation in $|\Lambda|$ as the point source position is varied in the streamwise direction, at constant y_0 . The strongest receptivity occurs for a position just marginally downstream of the trailing edge. Figures 4a and 4b correspond to the same value $y_0 = 0.1$, but the x_0 scale has been expanded in figure 4b. This figure clearly illustrates that the receptivity drops off exponentially for large positive x_0 , while it only drops off algebraically for large negative x_0 . Again, we see that upstream positions are more effective than downstream positions in exciting shear layer instability waves. Figure 4c presents the corresponding results for $y_0 = 0.25$. Although the transverse distance has more than doubled, there is only a modest decrease in the maximum receptivity level.

Next we present some results for a high subsonic Mach number, $M = 0.8$. The Receptivity Coefficient for an actuator on the outer surface of the splitter plate is presented in figure 5. The magnitude $|\Lambda|$ (figure 5a) at first drops off rather rapidly with upstream distance $|x_0|$, but the fall off quickly becomes more gradual, tending toward an asymptotic $|x_0|^{-1/2}$ behavior at large distances. For comparison, the instability wavelength is approximately $\lambda = 4.5$. Thus, the receptivity level decreases by approximately a factor of two when the actuator is moved one instability wavelength upstream. The reduced phase of the Receptivity Coefficient, which accounts for the time delay in an acoustic wave propagating from the actuator to the trailing edge, is plotted in figure 5b. The reduced phase is remarkably insensitive to the actuator location.

In figure 6, the corresponding results are presented for the receptivity to an actuator on the inner surface of the splitter plate in a Mach 0.8 flow. (The abscissa of the plot is reversed relative to figure 5.) The actuator size is approximately $\frac{1}{20}$ of the instability wavelength, and generates a circular arc deflection profile with a volume displacement equal to that for the external actuator considered in figure 5. Compared to the external actuator, the effectiveness of the actuator on the internal surface is increased much more significantly by proximity to the trailing edge. The reduced phase of the Receptivity Coefficient, which takes account of the time delay for downstream propagation in the moving stream, is plotted in figure 6b. The reduced phase has significant variations due to near-field effects in the region $(-x_0) < 2$, but becomes relatively constant at distances farther from the trailing edge.

Results for actuators on the outer and inner surfaces of the splitter plate for a Mach 1.5 flow are presented in figures 7 and 8. The behavior of the magnitude and phase of the Receptivity Coefficient for an external actuator on the supersonic flow is qualitatively similar to that for the subsonic case in figure 5. Again, a gradual monotonic decay in the receptivity level is observed as the actuator is moved further from the trailing edge. In contrast, the receptivity for the actuator on the internal surface in the supersonic flow (figure 8) exhibits significant differences from the corresponding subsonic case (figure 6). A distinctive modulation of the receptivity level occurs as the actuator location is varied in the supersonic case. This feature is due to variations in the constructive/destructive interference between the fast and slow supersonic waves, both of which travel downstream in the supersonic flow. The reduced phase plotted in figure 8b accounts for the time delay associated with the slow supersonic wave. The reduced phase in figure 8b approaches a constant (ignoring the modulation pattern), showing that the slow wave makes the dominant contribution to the receptivity. At higher Mach numbers, one would anticipate a more equal balance between the influence of the slow and fast waves, leading to stronger modulation of the pattern.

Finally, in figure 9 we present results for trailing-edge receptivity due to an incident plane acoustic wave for the case of a supersonic flow, $M = 1.5$. The variation of $|\Lambda|$ with respect to θ_0 bears a resemblance to the $\sin \frac{1}{2}\theta_0$ pattern found for low Mach numbers, but some distortion is present. The phase of Λ is seen to vary significantly as a function of the incidence angle.

5 Conclusions

A theoretical analysis has been presented for the excitation of shear layer instability waves by actuators which produce pressure (acoustic) fields. The results show that the shear layer is most receptive to actuators located near the trailing edge. Actuators downstream of the trailing edge are generally less effective than actuators upstream of the trailing edge, particularly when the distance from the trailing edge becomes of the order of or larger than the instability wavelength. Analyses have been developed for both subsonic and supersonic streams, and a number of interesting physical effects have been identified.

6 Appendix

The Wiener-Hopf technique requires a multiplicative factorization of the kernel function $K(\lambda)$, defined by (25), into the product of two functions,

$$K(\lambda) = K^+(\lambda)K^-(\lambda)$$

where $K^+(\lambda)$ and $K^-(\lambda)$ are analytic in the upper and lower halves of the complex plane, respectively. This multiplicative factorization is achieved by using the Cauchy integral formula

to obtain an additive decomposition of the function

$$L(\lambda) = \ln(K(\lambda)).$$

The Cauchy integral formula states

$$L(\lambda) = \frac{1}{2\pi i} \oint \frac{L(\zeta)}{\zeta - \lambda} d\zeta,$$

where the integral is evaluated around a closed contour that surrounds the pole at $\zeta = \lambda$ and contains no other singularities of $L(\zeta)$. We choose the point $\zeta = \lambda$ to lie in the strip of overlap between the lower and upper half-planes for the Wiener-Hopf analysis, and the contour to be a 'generalized rectangle' within this same region consisting of two long horizontal sides that pass above and below the pole, and two short connecting vertical segments. The form of the function $K(\lambda)$ was chosen so that it approaches one as $\lambda \rightarrow \pm\infty$ in the strip. Thus, when we deform the integration contour so that the two long horizontal segments extend from $-\infty$ to ∞ , the contributions from the two vertical segments vanish. We can then write

$$L(\lambda) = L^+(\lambda) + L^-(\lambda)$$

where the plus and minus functions correspond to the contributions from the two horizontal segments of the contour,

$$L^+(\lambda) = \frac{1}{2\pi i} \int_{-\infty}^{\infty} \frac{L(\zeta)}{\zeta - \lambda} d\zeta \quad \text{and} \quad L^-(\lambda) = \frac{-1}{2\pi i} \int_{-\infty}^{\infty} \frac{L(\zeta)}{\zeta - \lambda} d\zeta$$

and the contours of integration for $L^+(\lambda)$ and $L^-(\lambda)$ pass below and above the pole at $\zeta = \lambda$, respectively. The multiplicative factorization of $K(\lambda)$ is then given by

$$K^+(\lambda) = \exp(L^+(\lambda)), \quad K^-(\lambda) = \exp(L^-(\lambda)).$$

The procedure for calculation of the additive split of $H(\lambda)$ follows directly from the Cauchy integral formula,

$$H^+(\lambda) = \frac{1}{2\pi i} \int_{-\infty}^{\infty} \frac{H(\zeta)}{\zeta - \lambda} d\zeta \quad \text{and} \quad H^-(\lambda) = \frac{-1}{2\pi i} \int_{-\infty}^{\infty} \frac{H(\zeta)}{\zeta - \lambda} d\zeta,$$

where the contours of integration for $H^+(\lambda)$ and $H^-(\lambda)$ pass below and above the pole at $\zeta = \lambda$, respectively.

References

- [1] Parekh, D.E., Kibens, V., Glezer, A., Wiltse, J.M., & Smith, D.M. 1996 Innovative jet flow control: mixing enhancement experiments. AIAA 96-0308.
- [2] Cain, A.B. 1995 Numerical simulation of trailing edge receptivity. Bull. Am. Phy. Soc. 40 , 2025.
- [3] Morgan, J.D. 1974 The interaction of sound with a semi-infinite vortex sheet. Q. J. Mech. Appl. Math. 27 , 465-487.
- [4] Munt, R.M. 1977 The interaction of sound with a subsonic jet issuing from a semi-infinite cylindrical pipe. J. Fluid Mech. 83 , 609-640.
- [5] Munt, R.M. 1990 Acoustic transmission properties of a jet pipe with subsonic jet flow: I The cold jet reflection coefficient. J. Sound Vib. 142 , 413-436.
- [6] Cargill, A.M. 1982 Low frequency sound radiation and generation due to interaction of unsteady flow with a jet pipe. J. Fluid Mech. 121 , 59-105.
- [7] Pal, A. 1996 Receptivity of a supersonic cylindrical jet to an acoustic wave. Part I - Solution based on the Wiener-Hopf technique. Forum on High Speed Flows, ASME Fluids Engineering Conference, San Diego, 7-11 July.
- [8] Bower, W.W. & Pal, A. 1996 Receptivity of a supersonic cylindrical jet to an acoustic wave. Part II - Numerical results. Forum on High Speed Flows, ASME Fluids Engineering Conference, San Diego, 7-11 July.
- [9] Noble, B. 1958 Methods Based on the Wiener-Hopf Technique. Pergamon.
- [10] Crighton, C.G. 1985 The Kutta condition in unsteady flow. Ann. Rev. Fluid Mech. 17, 411-445.
- [11] Peake, N. 1994 The viscous interaction between sound waves and the trailing edge of a supersonic splitter plate. J. Fluid Mech. 264, 321-342.

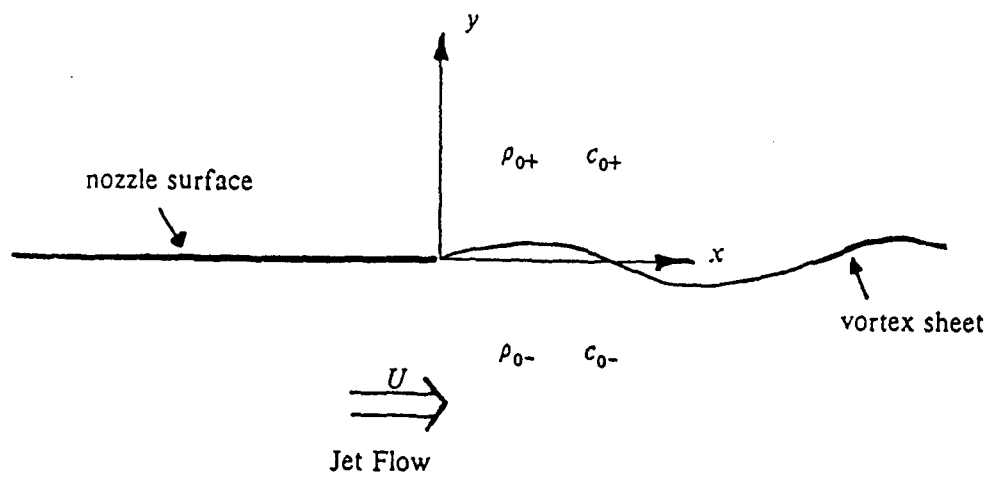


Fig. 1. A sketch of the geometry and coordinate system.

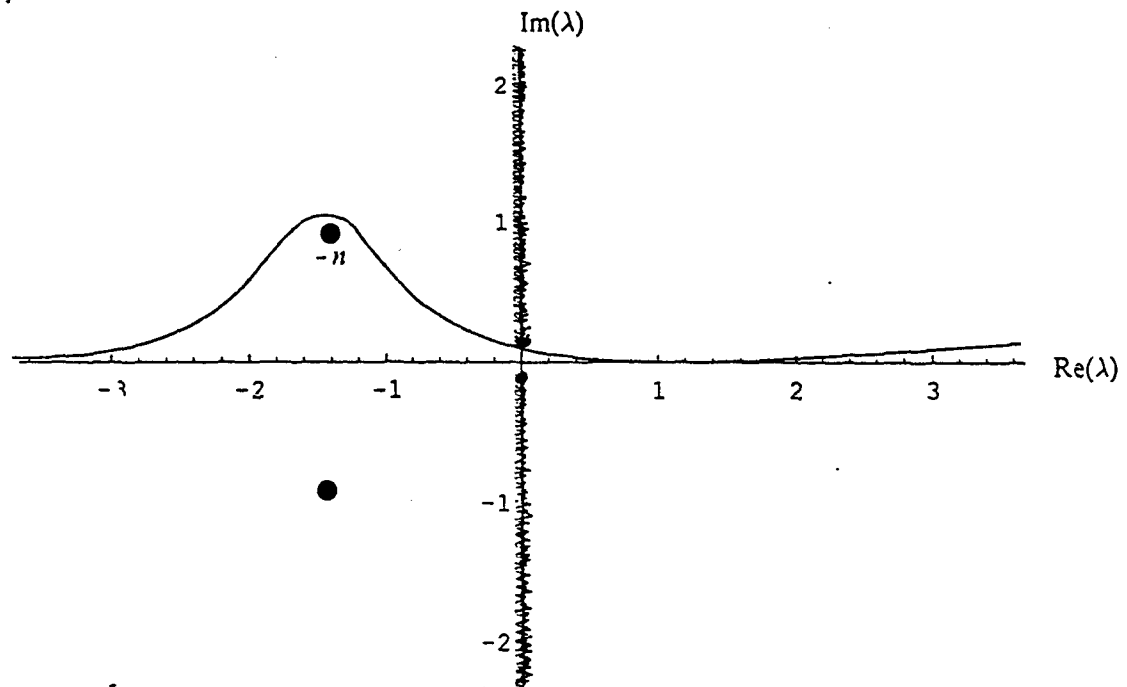


Fig. 2. An illustration of the singularities (branch points and poles) in the complex λ -plane and the transform inversion contour. (a) $M = 0$.

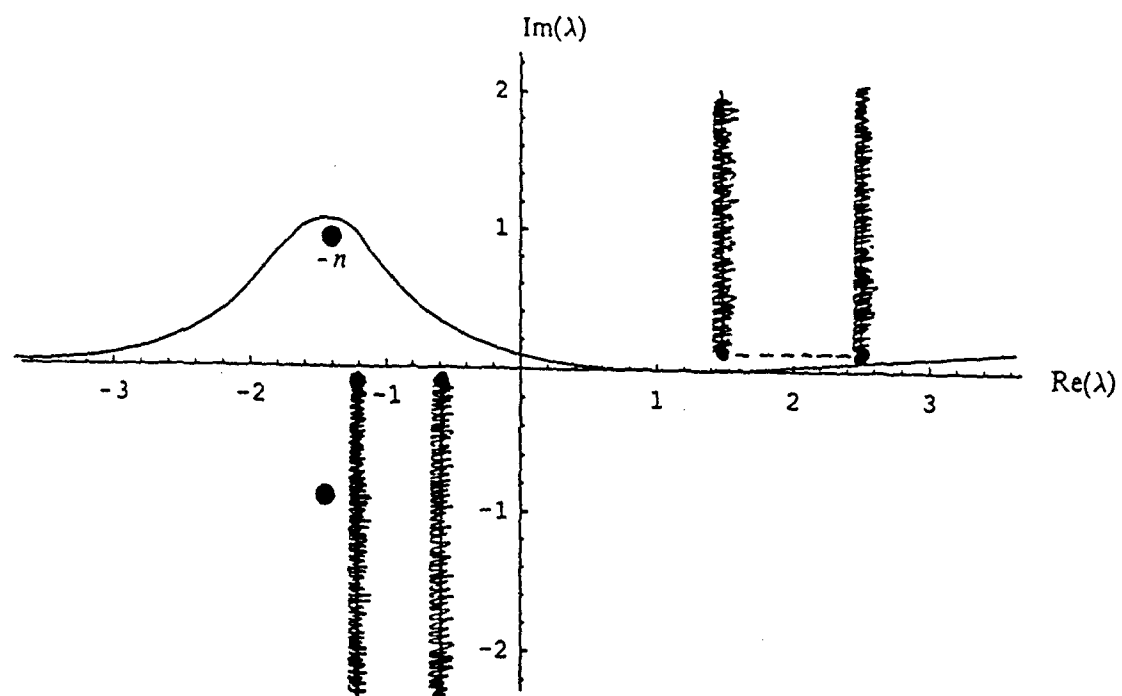


Fig. 2. An illustration of the singularities (branch points and poles) in the complex λ -plane and the transform inversion contour: (b) $M < 1$.

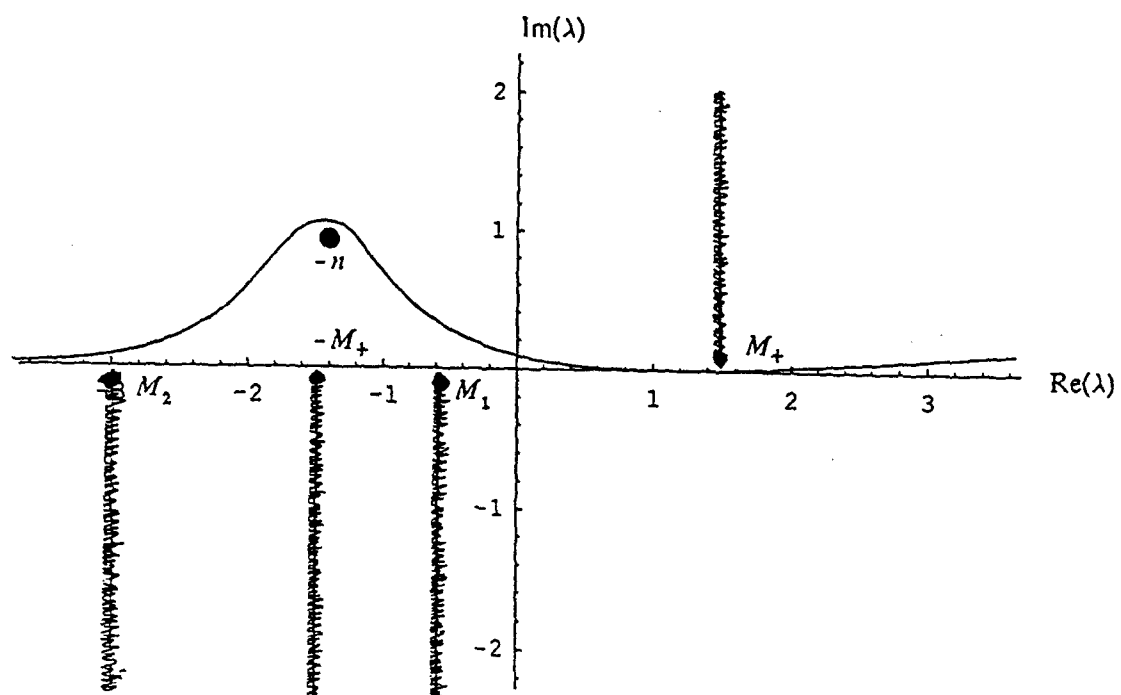


Fig. 2. An illustration of the singularities (branch points and poles) in the complex λ -plane and the transform inversion contour: (c) $M > 1$.

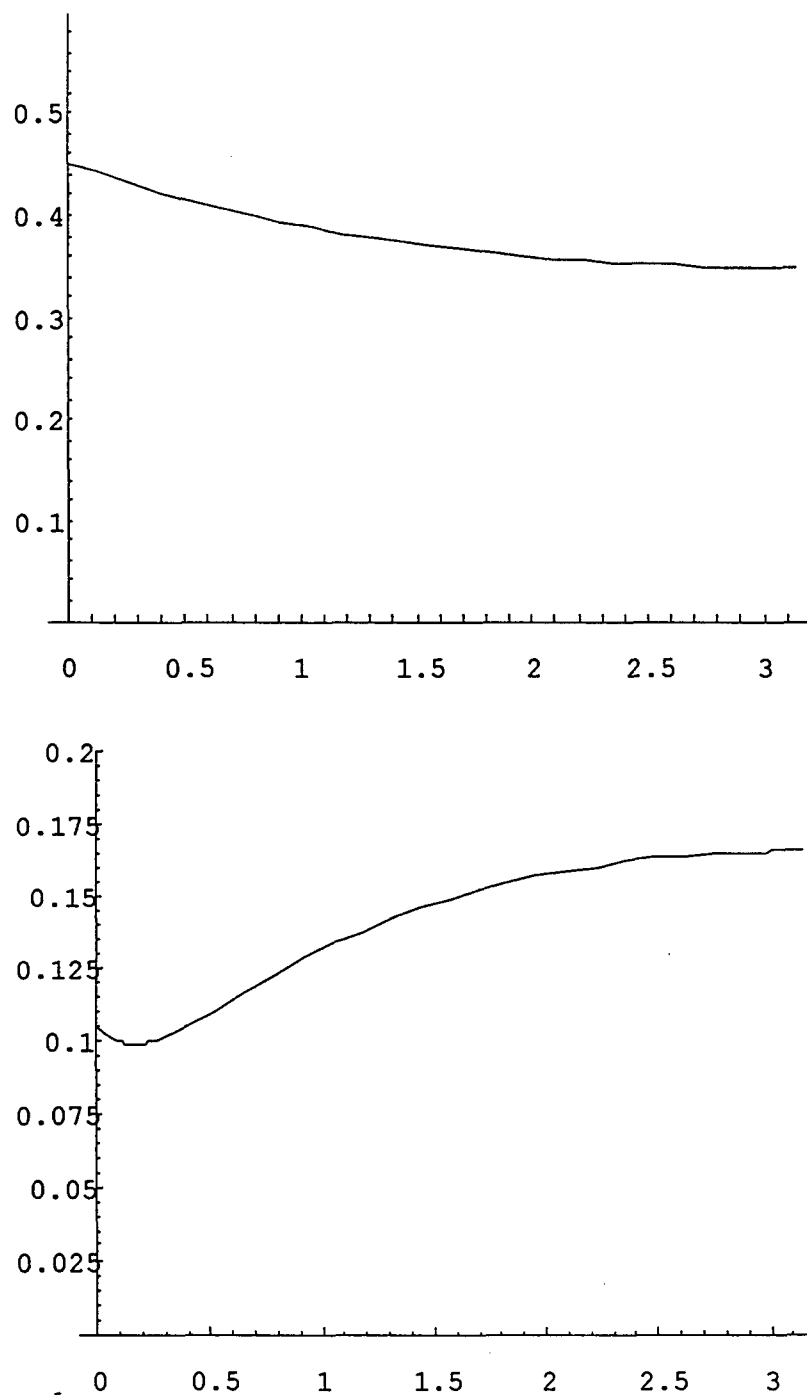


Fig. 3. Magnitude $|\Lambda|$ of the Receptivity Coefficient for a point source at the polar location (r_0, θ_0) outside the stream, with $M = 0$. Values plotted as a function of θ_0 : (a) $r_0 = 0.1$; (b) $r_0 = \frac{1}{2}\pi$.

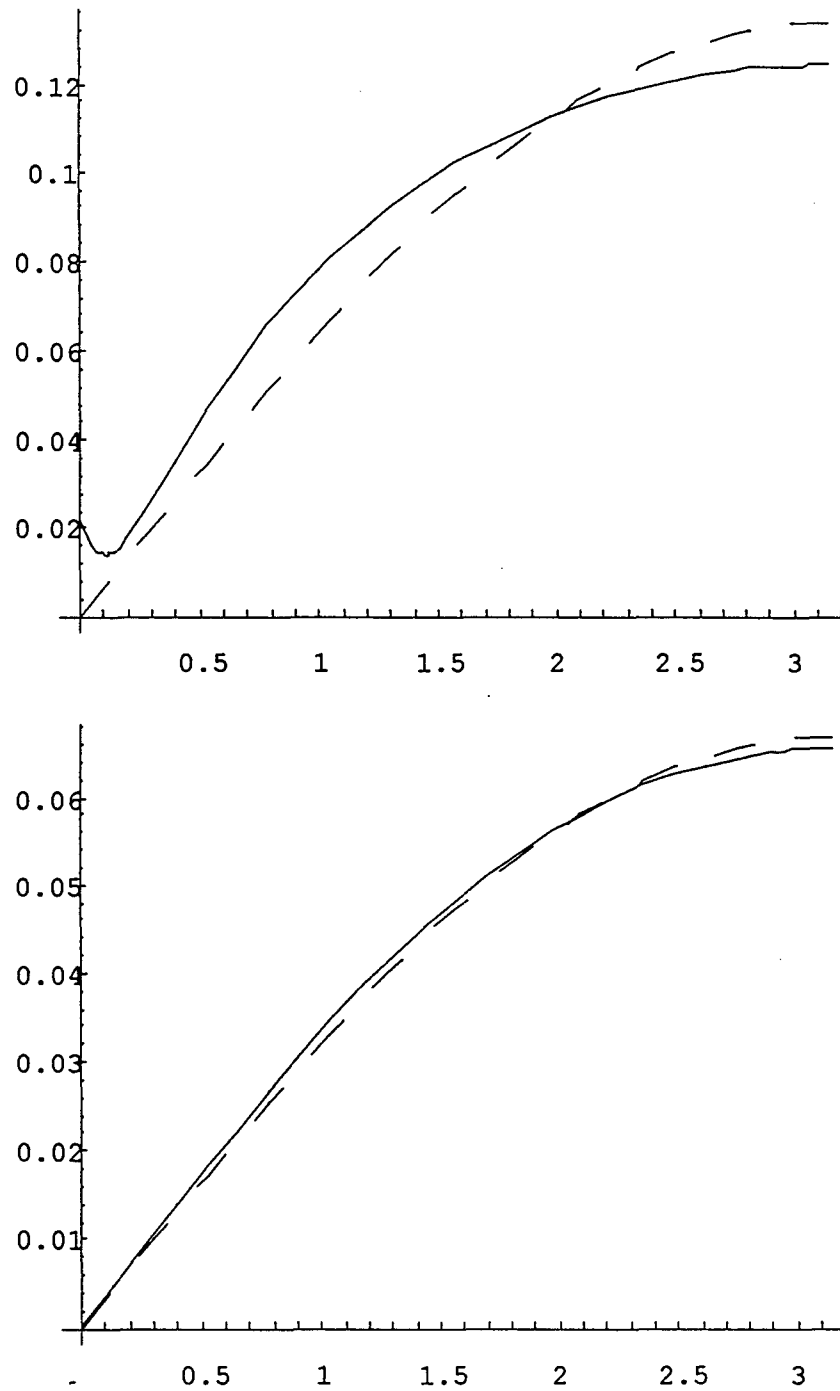


Fig. 4. Magnitude $|\Lambda|$ of the Receptivity Coefficient for a point source at the polar location (r_0, θ_0) outside the stream, with $M = 0$. Values plotted as a function of θ_0 : (a) $r_0 = \pi$; (b) $r_0 = 4\pi$.

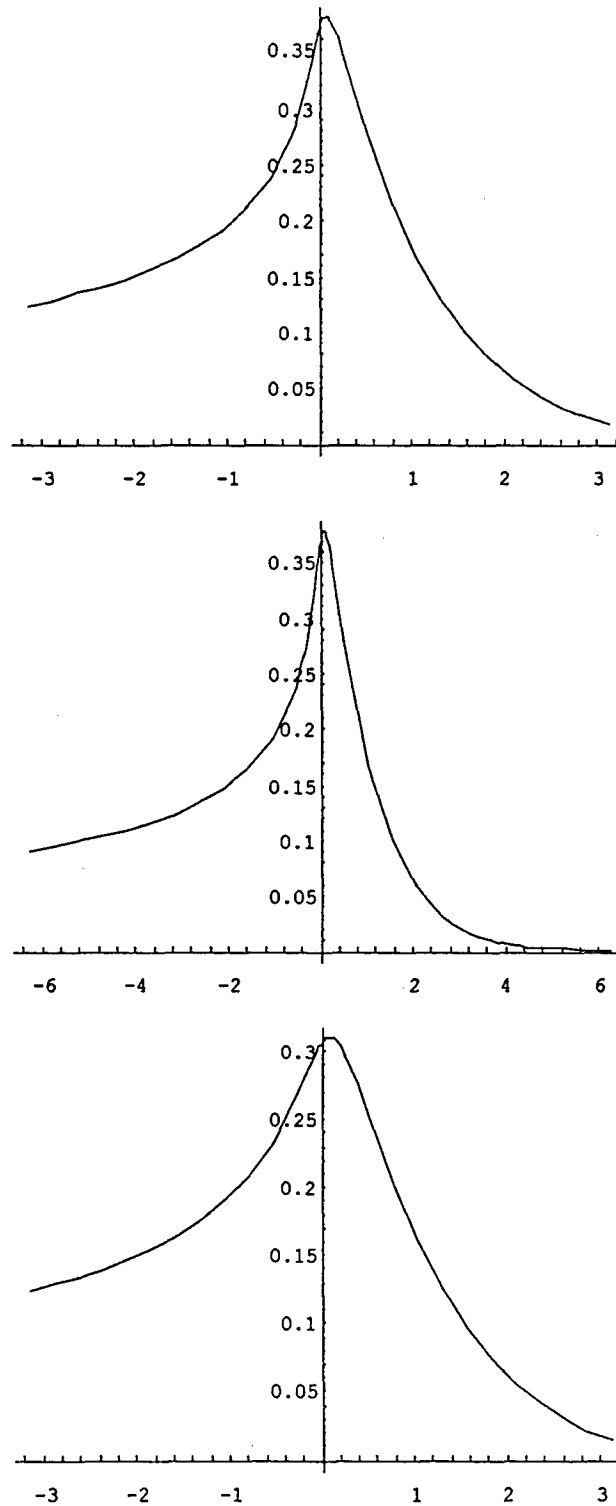


Fig. 5. Magnitude $|\Lambda|$ of the Receptivity Coefficient for a point source at the location (x_0, y_0) outside the stream, with $M = 0$. Values plotted as a function of x_0 : (a) $y_0 = 0.1$, $-\pi < x < \pi$; (b) $y_0 = 0.1$, $-2\pi < x < 2\pi$; (c) $y_0 = 0.25$, $-\pi < x < \pi$.

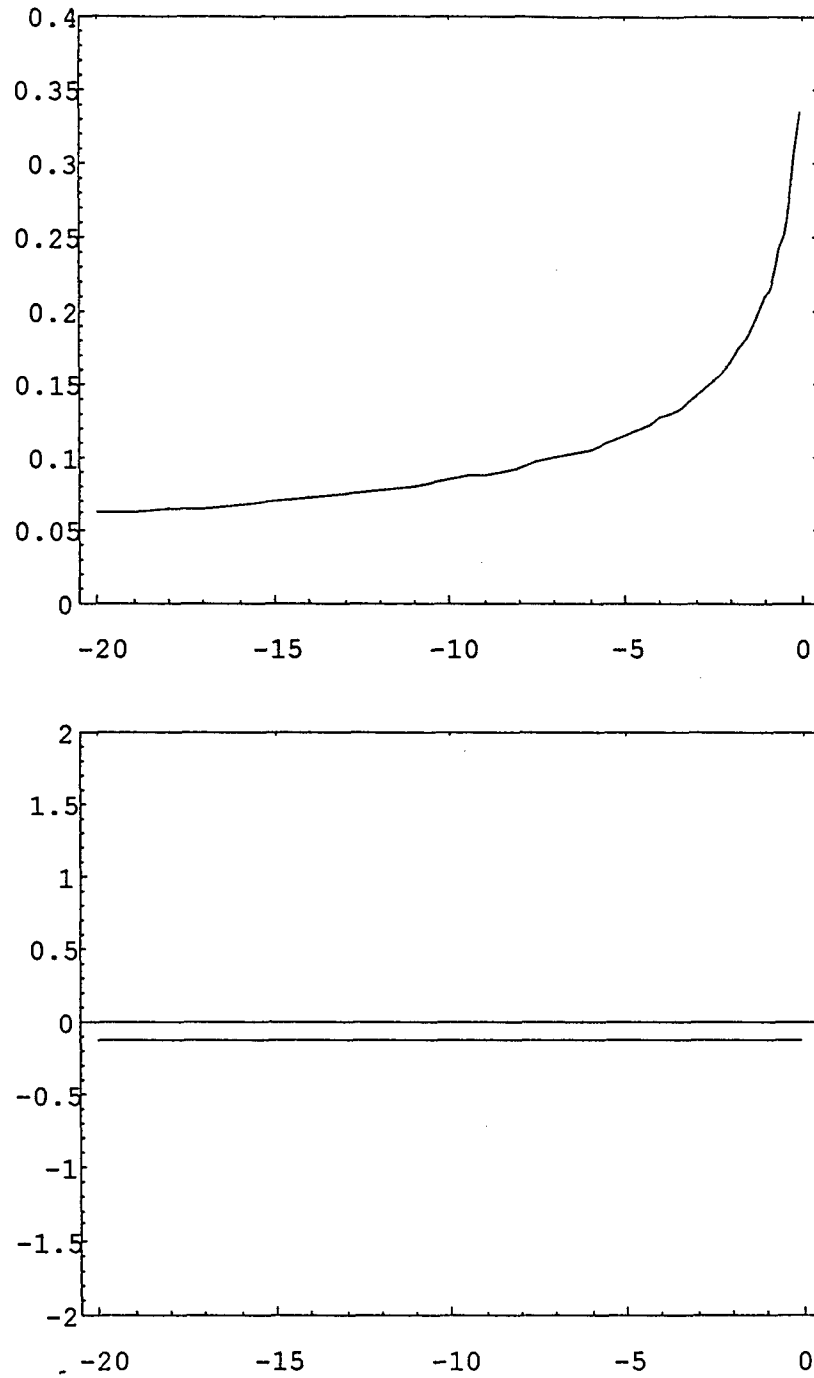


Fig. 6. Receptivity Coefficient for an actuator on the external surface ($y = 0+$) of the splitter plate, as a function of actuator location x_0 , with $M = 0.8$: (a) the magnitude, $|\Lambda|$; (b) the reduced phase, $\arg[\Lambda \exp(iMx_0)]$.

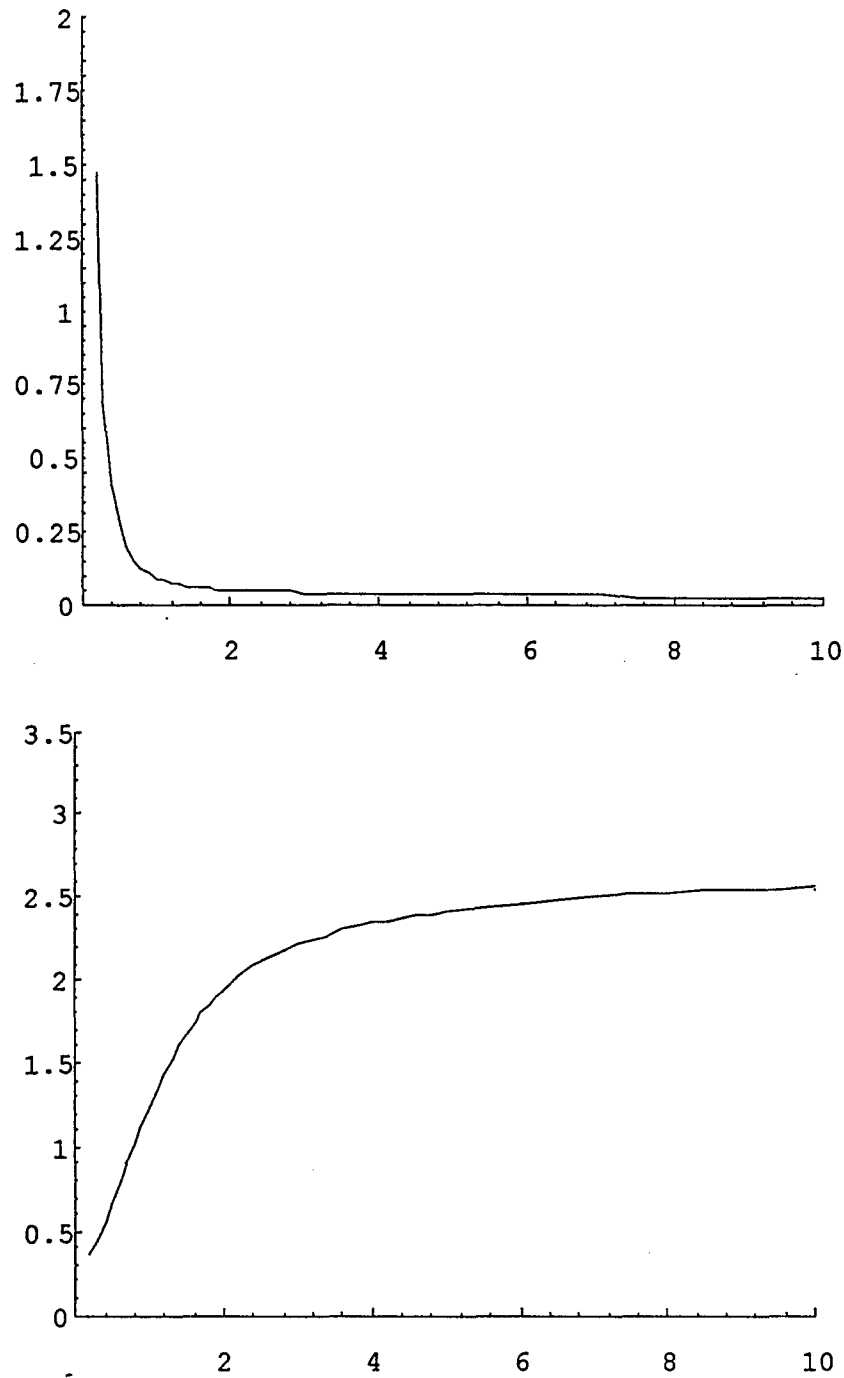


Fig. 7. Receptivity Coefficient for an actuator on the internal surface ($y = 0-$) of the splitter plate, as a function of actuator location x_0 , with $M = 0.8$: (a) the magnitude, $|\Lambda|$; (b) the reduced phase, $\arg[\Lambda \exp(iMLx_0/(1+M))]$.

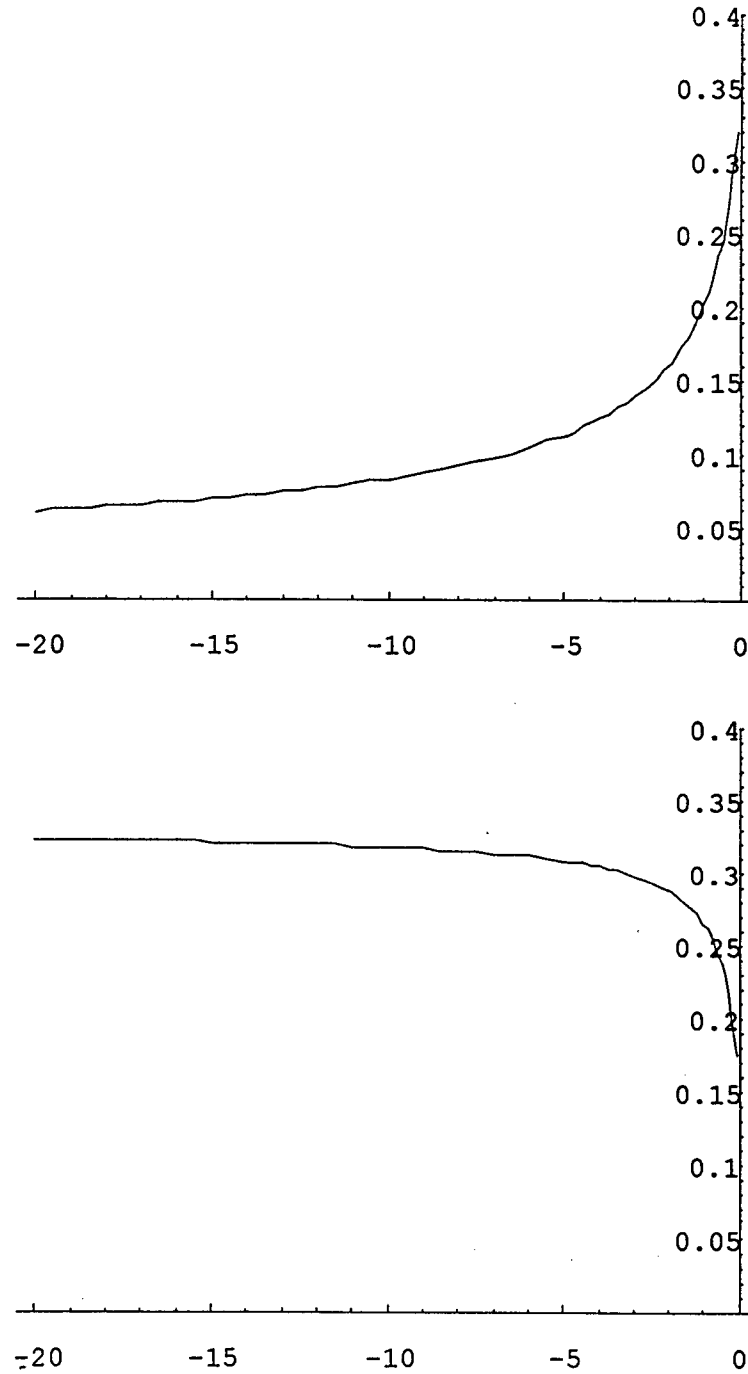


Fig. 8. Receptivity Coefficient for an actuator on the external surface ($y = 0+$) of the splitter plate, as a function of actuator location x_0 , with $M = 1.5$: (a) the magnitude, $|\Lambda|$; (b) the reduced phase, $\arg[\Lambda \exp(iMx_0)]$.

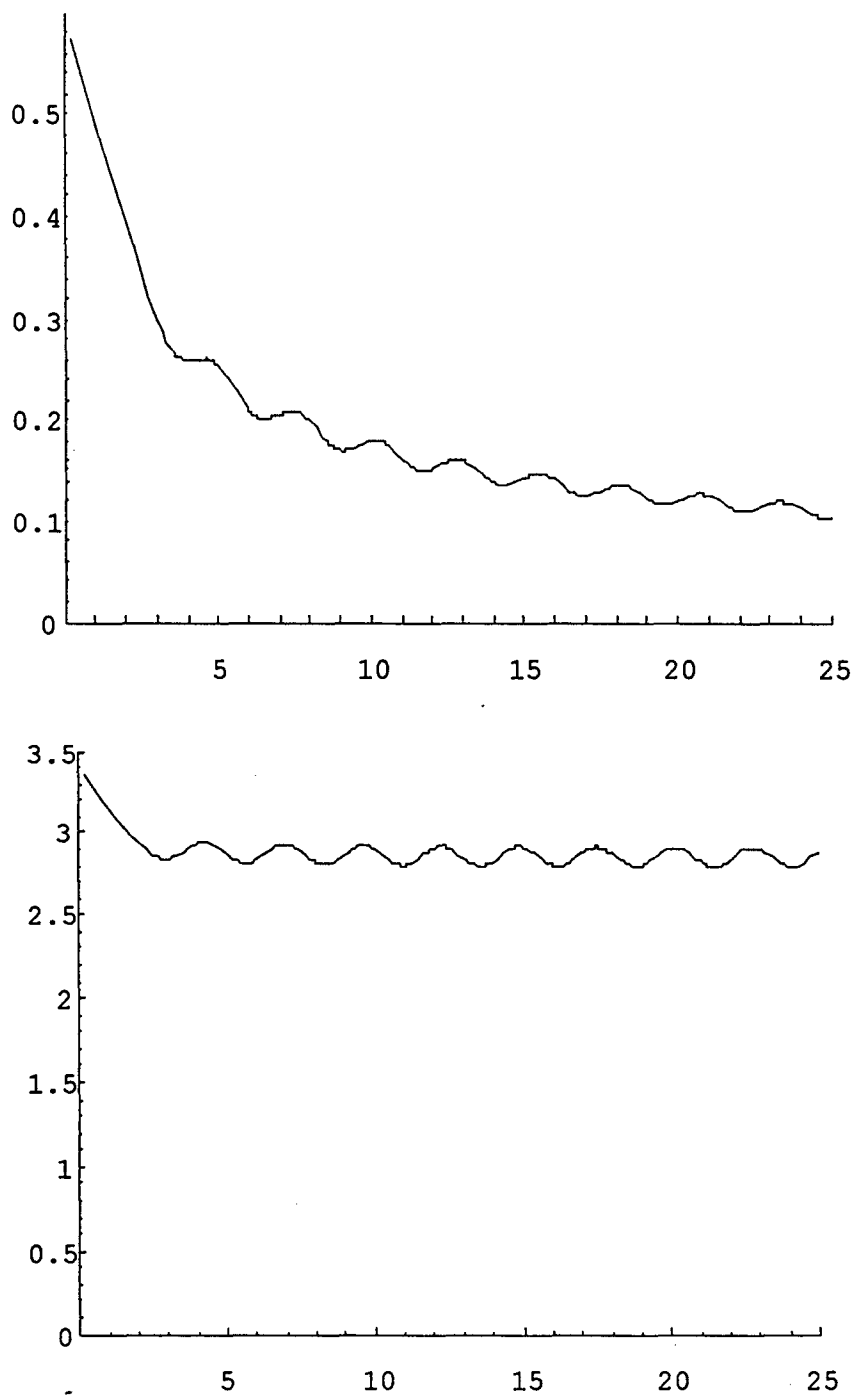


Fig. 9. Receptivity Coefficient for an actuator on the internal surface ($y = 0-$) of the splitter plate, as a function of actuator location x_0 , with $M = 1.5$: (a) the magnitude, $|\Lambda|$; (b) the reduced phase, $\arg[\Lambda \exp(iMLx_0/(M-1))]$.

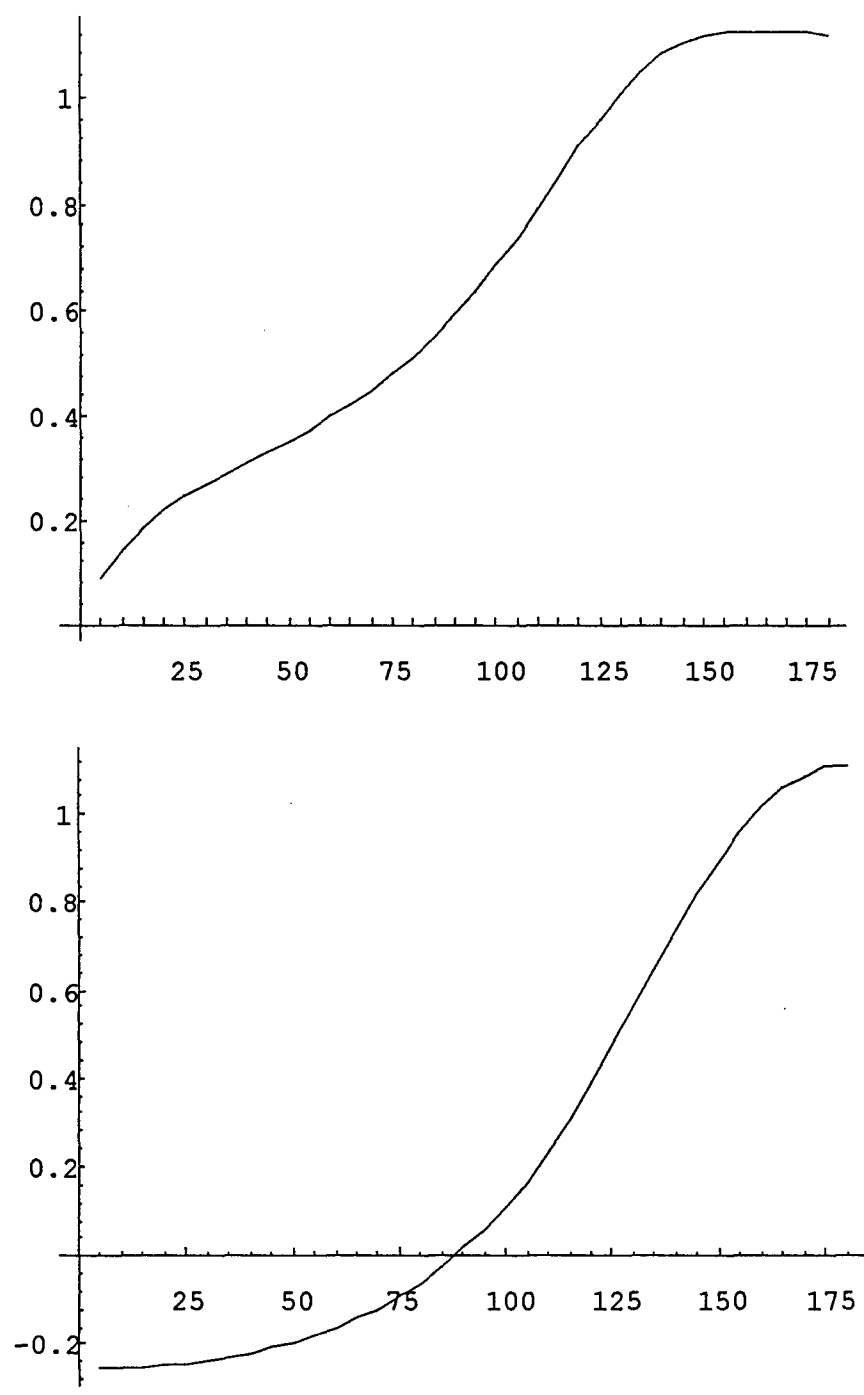


Fig. 10. Receptivity Coefficient for an acoustic plane wave incident on the trailing-edge from the direction θ , $M = 1.5$: (a) the magnitude, $|\Lambda|$; (b) the phase, $\arg(\Lambda)$.